Evaluating hazards at salt cavern sites using multichannel analysis of surface waves

Julian Ivanov, Kansas Geological Survey
Birgit Leitner, Fugro, Austria GmbH, formerly University of Leoben
William Shefchik, Burns and McDonnell Engineering Company
J. Tyler Shwenk and Shelby L. Peterie, Kansas Geological Survey

Subsidence resulting in sinkholes within dissolution mine fields in and around the city of Hutchinson, Kansas, USA (Figure 1) has been reported for more than 90 years. Salt dissolution and the resulting unpredictable upward migration of the dissolution voids can be observed both in proximity to well bores (dissolution mining, brine disposal, and oil wells; seismic shot holes, etc.) and in areas known to experience natural dissolution with no apparent anthropogenic influences. One potential outcome of the upward migration of these long-inactive dissolution voids in the city of Hutchinson is significant structural damage to facilities, infrastructure, or traffic areas. Monitoring the condition of a void's roof is key to determining and managing this risk. Drilling is expensive for this investigative application in part because of the number of potential targets. At a depth of approximately 120 m, most surface geophysical methods have neither the sensitivity nor resolution necessary to detect these voids, much less interrogate the roof.

From the shear modulus (stress/strain relationship), rock failure can be loosely predicted from the stress/strain curve. Because shear velocity is proportional to the shear modulus, increases in rock stress translate to increases in shear velocity. Therefore, the likelihood of failure of a void's roof increases as the measured shear-wave velocity increases in the roof rock. Measuring shear velocity noninvasively in this urban setting and at these depths would be extremely challenging using any active seismic method. Considering the objectives and the site, the passive multichannel analysis of surface waves (MASW) method was determined to possess the greatest potential for successfully meeting the project objectives.

Prioritizing production borings at this former mine site allows voids under the greatest relative roof stress to be stabilized first, thereby minimizing the chances of an unexpected surface failure to occur during a multiyear reclamation process. With the depth of salt at approximately 125 m and a key structural layer (interbedded dolomite) at about 70 m below ground surface, dispersive surface waves with frequencies down to around 3–5 Hz are necessary to sufficiently sample at and immediately below this key 70-m dolomite. Active MASW sources did not possess the required low frequencies and, in this noisy setting, they also did not have the necessary energy levels to meet the survey requirements. By using a passive approach to MASW and principally noise from passing trains as an energy source, sampling depths in excess of 70 m were observed and the method was effective in identifying anomalous shear-wave velocity increases as small as 10%. Follow-up borings and logs verified the accuracy of this method for identifying voids that had migrated to or above the salt-shale contact, and a few voids that had migrated to the dolomite layer.

Introduction

Extensive solution mining of the Permian Hutchinson Salt Member has been ongoing for more than a century in and around Hutchinson, Kansas. The Hutchinson salt occurs in

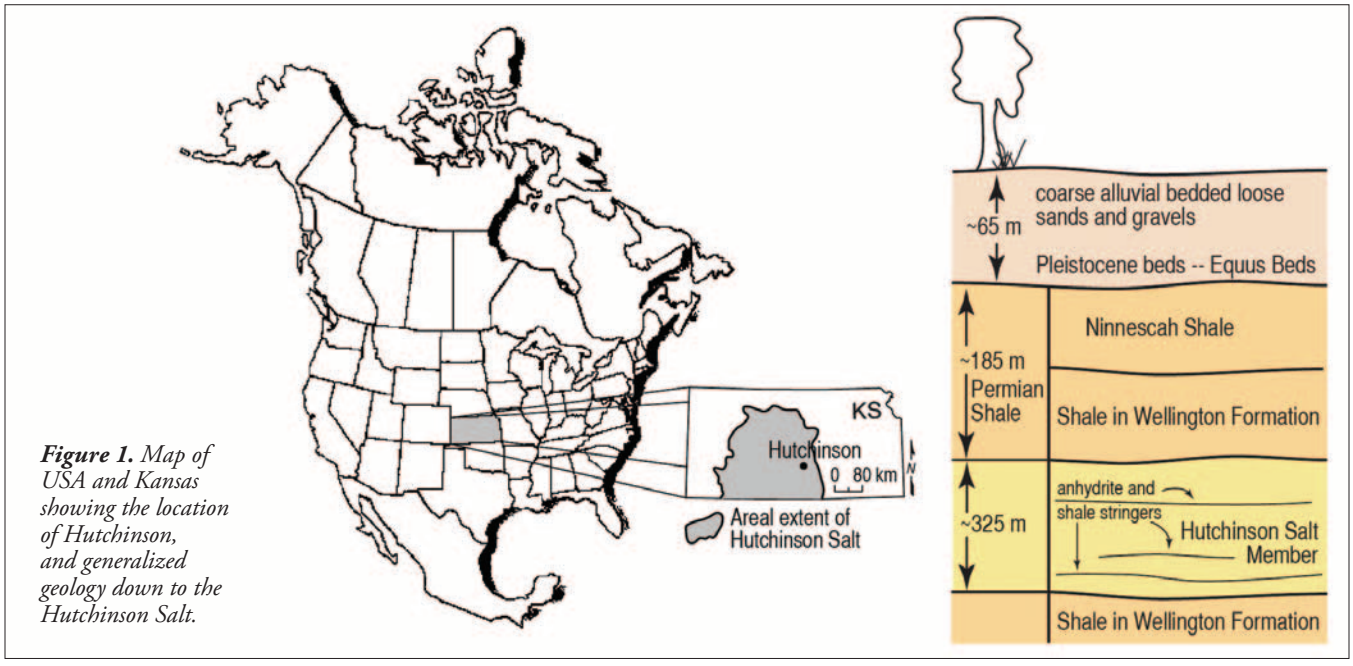

Figure 1. *Map of USA and Kansas showing the location of Hutchinson, and generalized geology down to the Hutchinson Salt.*

central Kansas, northwestern Oklahoma, and the northeastern portion of the Texas Panhandle, and is prone to and has an extensive history of dissolution and formation of sinkholes (Figure 1). In Kansas, the Hutchinson Salt Member possesses an average net thickness of 80 m and reaches a maximum of more than 150 m in the southern part of the basin. Mining practices in the early 20th century lacked control over the development of the dissolution void, which many times resulted in the removal of the salt up to the base of the overlying shale. The lack of a salt roof can result in the upward migration of the void into the shale cap overlying the salt.

When the roof rock of an undersupported void fails, vertical growth moves progressively upward layer-by-layer through the overburden as stress exceeds the strength of each successive undersupported span of new roof rock. The void space available to accommodate roof-collapse material and stress on the overburden are key characteristics determining whether void movement is possible through the entire overburden-rock column.

Borehole studies at well sites included borehole logs (electric and lithologic), sonar surveys of the key voids, and acoustic televiewer logs. These data provided excellent information about the current condition of the voids and the characteristics of the near-borehole materials.

Anomalous shear-wave velocity (V_s) is a key indicator of either previous subsidence activity or areas where voids have a strong potential for roof collapse. Lateral decreases in V_s are related to failure and localized increases in V_s are associated with the tension dome surrounding subsurface cavities (Davies, 1951) (Figure 2). Confidently mapping the subsidence geometry depends on the abruptness of the contrast (gradient) between the disturbed and undisturbed earth materials, the geometry, dimensions, and depth of the anomaly, and characteristics of seismic-source energy.

Several key characteristics of surface waves and surface-wave imaging make application of this technique possible in areas and at sites where other geophysical tools have failed or provided inadequate results. First and most important is the ease with which surface waves can be generated. The relatively high-amplitude nature of surface waves in comparison to body waves makes their application possible in areas with elevated levels of mechanic/acoustic noise. The final products of the surface-wave method are V_s estimates with depth. Still, the active surface-wave method is applicable only to the shallow portion of the near surface and the maximum depth of penetration is strongly dependent on the lowest frequencies (i.e., longest wavelengths) that can be generated and recorded at a specific site. For example, when using active seismic sources, it is common to obtain V_s estimates down to ~30 m and when using passive sources down to ~100 m (or more depending the nature of the source).

The MASW method uses multichannel seismic data acquired in a roll-along manner along a profile line (Miller et al., 1999). Each record is acquired at a different shot station along the profile line and is transformed into a unique phase-velocity—frequency domain image (Park et al., 1998). From that image, a fundamental-mode (most often) dispersion curve is interpreted and estimated. Each dispersion curve is inverted into a 1D V_s profile (Xia et al., 1999), and all 1D V_s profiles sutured together into a 2D V_s cross section (Miller, et al., 1999).

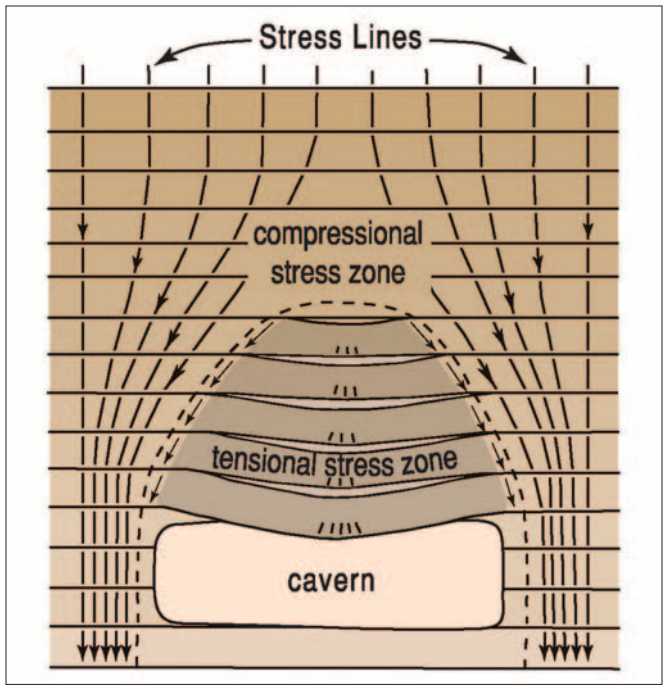

Figure 2. *Tension dome and distribution of stress lines around a cavern opening in horizontal strata (modified from Davies, 1951).*

Surface-wave tests were performed to determine how to optimally record low-frequency surface waves sufficient to fully sample the upper 70 m. Based on theory, localized increases in shear-wave velocity along the bedrock surface could be an indicator of subsidence potential. As previously indicated, frequencies in the 3–5 Hz range would be necessary to uniformly interogate to depths of 70 m or more at this site. Unfortunately, the material characteristics of the weak shale at this site made producing frequencies below 10 Hz with traditional active sources difficult. Ultimately, that limitation hindered sampling the shear-wave velocity within the overburden.

Passive 2D array

Passive surface-wave recording allows random sources of seismic energy (trains, manufacturing facilities, heavy vehicles on roadways, processing plants, heavy construction equipment, etc.), normally considered noise on active surveys, to be used with data-processing enhancements and specialized methods to calculate 1D shear-wave velocity functions (Louie, 2001; Park et al., 2007).

Preliminary testing using a simple uniform 2D spread of receivers at the site verified sufficient and acceptable seismic energy was generated by trains from three principal directions relative to the 2D grid of receivers (north, west, and east). The recorded passive seismic energy included frequencies well below 5 Hz.

Next, an irregular 2D receiver grid with variable receiver and line spacing was designed based on data recorded from

the uniform 2D spread (Figure 3). This spread was unique and was tailored to this site and distribution of source energy. The spread proved effective in recording seismic energy with a near-optimal bandwidth and amplitude for interrogating earthen material between the 70-m dolomite and the 20-m deep bedrock surface at both well locations. The 336 receivers that composed this irregular grid made possible hundreds of orientations and grouping of receivers to gather and analyze dispersive characteristics. Preliminary testing on a large number of these different array sets provided results which strongly support the reconnaissance potential and value of this approach.

Data acquisition. The 336 receiver stations were occupied by single 4.5-Hz geophones (Figure 3) and recorded on a distributed Geometrics Geode seismograph system. Data were recorded at a 2-ms sampling interval resulting in 16,000 samples per trace for a 32-s listen time. The seismographs were manually triggered in response to both visual and audible indications when a train was within recording distance. Several hundred individual 32-s, 336-channel seismograms were recorded throughout the night.

Data processing. Processing the grid-style data like that recorded for this survey follows the basic principles developed by scientists at the Kansas Geological Survey (KGS) and others who have been successful using passive surface-wave data to estimate the deep (>30 m) V_s field. Spreads with a range of geometries were evaluated with different sets of optimum spreads defined for dispersion and inversion at each depth slice. The 1D velocity functions populated a volume generally above the target void as defined by invasive sonar interrogation. This V_s volume was then sliced at different depths for comparison and analysis.

Results. Analysis of thousands of different array configurations allowed confidence in the depth-slice velocity profiles at wells 40 (where a cavern void was known to be present in the shale) and 94 (where it was known from drilling that no cavern void was present in the shale). V_s estimates from both sites carried a low percentage error relative to measurement confidence and consistency. Subarrays centered on nine different locations around the 2D spreads were used to define the dispersions curves and then invert for V_s as a function of depth. The depth interval along each trace was divided into 12 layers, providing directly comparable velocity functions.

Summing the average velocity from all nine V_s functions calculated for each well location allowed comparison of general velocity trends. Evaluation of velocity curves and percentage difference for these two data sets strongly suggests the method consistently detected higher V_s for well 40 (where the void is known to be at the base of the dolomite), and values were consistent with local background velocities in well 94 (where the void is well down into the salt) (Figure 4). With an average velocity approximately 10% lower below the eighth layer at well 94 relative to well 40 and with the shallowest five layers all possessing statistically identical values, observations and ascertainments based on the passive surface-wave data match the predictions based on the elastic moduli. The relatively elevated velocities beneath well 40 are likely indicative of elevated stress that is still below the failure point of rocks currently providing the roof for the upward-migrating void.

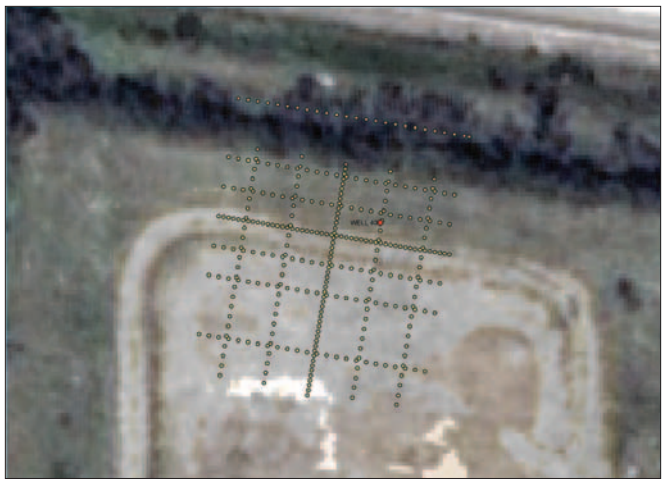

Figure 3. *Irregular 2D receiver grid overlaying orthophoto of well 40 site.*

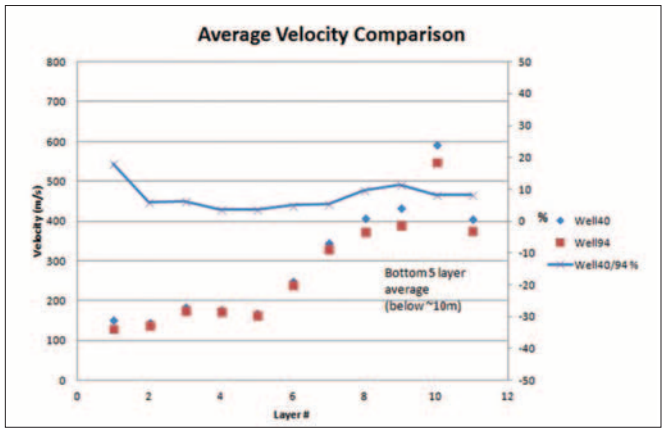

Figure 4. *Comparison of average velocity at each layer for the two well sites. The blue line defines the percentage difference between velocities calculated for each well site.*

Confident measurements of V_s could be made to depths in excess of 40 m. Comparisons of V_s calculated for the lower depth intervals at both well sites provided the basis for a compelling argument supporting the assertion that this type of passive monitoring is capable of discerning upward distribution of stress in advance of roof failure and collapse in these salt jugs between the dolomite and bedrock surface.

Passive linear (1D) array

Continuing the previous line of research at this site, a single long line of receivers was positioned as near target wellheads 94, 36, 33, 26, 25, 20, 19, 16B, 6A, and 5A as possible (Figure 5). Using train source energy and this single 1D alignment of receivers parallel to the railroad tracks, data were recorded in hopes of identifying void roofs with elevated shear velocity and therefore an increased risk of upward migration. Key to the success of this study was capturing train noise at the optimal offset from the profile and at night when all other cultural noise was minimal.

The most significant outcome of this study was the estimation and ordering of subsidence potential based on shear-velocity values in the roof rock of jugs along the northern boundary of the property. As a result, if an accurate estimate of shear velocity could be measured in roof rock from passively acquired data, this study could influence the order in which each jug along this 1D profile was remediated.

Data acquisition. This > 1 km profile was instrumented with 400 individual 4.5-Hz geophones spaced every 2.4 m and recorded on a Geometrics Geode distributed seismic system. The 32-s data were recorded using a 2-ms sampling interval. Consistent with the previous passive seismic survey at this site (e.g., at wells 40 and 94), the seismic energy was uncontrolled and provided by local sources. Analysis of the previous seismic energy sources captured during passive recording at this site clearly indicated trains from a distance as great as 5 km provided the best broad-spectrum, low-frequency seismic energy. Therefore, trains travelling predominantly EW and WE were the sources for this linear spread of receivers.

A small 2D grid of receivers was also deployed in a central location to allow energy alignment studies. These studies were instrumental in this and future studies where linear noise sources, like trains, are not available and industrial noise from variable and mobile sources must be recorded. The 2D spread/grid included 48 receivers in the form of a cross.

Data processing. Data were processed using several algorithms developed at the KGS in association with SurfSeis software. The method provided good quality results for this site. Unlike the previous study where a 2D grid was used and a wide range of sources was analyzed, this study used a 1D spread of receivers and only trains from distances optimal for the site were included in the analysis. At the same time, the 2D grid was used to monitor for and identify other possible passive sources that could interfere (e.g., when not aligned with the 1D line) with the analysis. This approach dramatically improved dispersion-curve analysis and minimized the standard deviation.

Seismic records (Figure 6) with optimal train energy, as defined by dispersion-curve images, with optimal

Figure 5. *Approximate location of 1D receiver spread targeting the northernmost wells at the Viginductries Inc. site.*

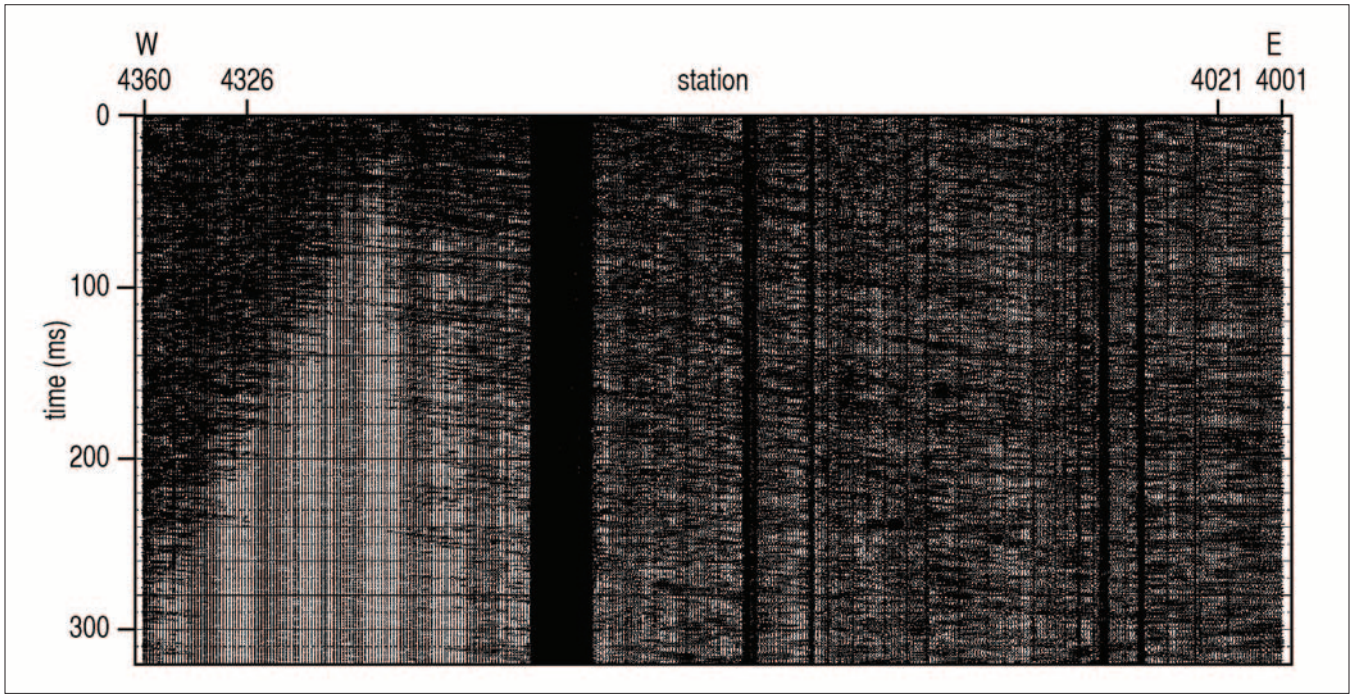

Figure 6. *Recorded passive seismic data using trains as seismic sources.*

signal-to-noise ratios were selected for analysis. Data were analyzed to find the ideal spread length which was based on two contradictory goals—to have as long a spread as necessary to fully sample low frequencies but as short as possible to maximize lateral resolution. It was estimated that the lowest recordable frequency was ~3 Hz and shortest spread that could record it would be ~250 m. Thus, from each record, 33 subspreads were extracted.

Results. Dispersion-curve images possessed low- and high-velocity patterns (Figure 7); key to penetration depth is energy below ~5 Hz. An approximation formula can be used for quick assessment of investigation depth and velocity. The ratio of velocity over frequency gives a wavelength half of which is equal to the approximate depth of investigation. For example, using Figure 7a, the velocity at 4 Hz is about 440 m/s; 440 / 4 = 110-m wavelength and 110 / 2 = 55 m depth.

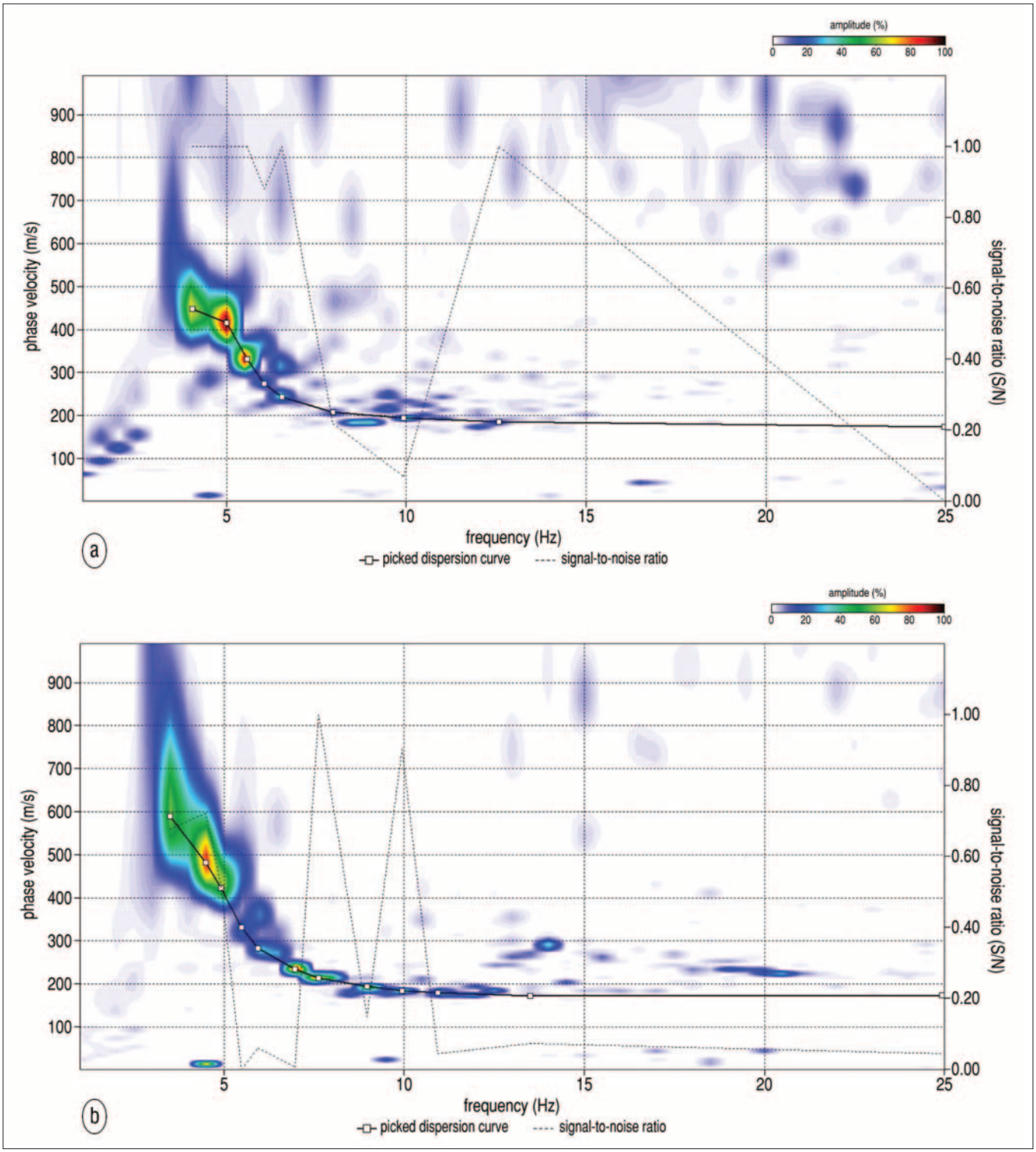

Figure 7. *Dispersion-curve images obtained from passive seismic data showing relatively low (a) or high (b) velocities at low frequencies (below 5 Hz) at horizontal locations 180 and 280.*

Thus, it can be approximated that the velocity at 55 m depth is 440 m/s. Similarly for Figure 7b, velocity at 4 Hz is about 520 m/s; 520 / 4 = 130-m wavelength and 130 / 2 = 65 m depth. Thus, it can be approximated that the velocity at 65 m depth is 520 m/s.

Dispersion curves were estimated from the overtone images. Each curve was inverted into a 1D V_s profile. All 1D profiles were assembled into a 2D image. The final 2D V_s section (Figure 8) did not include V_s from the bottom layers (i.e., half-space representation) of the 1D inversion estimates. This was done to minimize instability and generalization errors.

Relatively high-velocity zones were detected above all voids that currently have migrated into the shale overburden (Figure 8; five wells). No relatively high-velocity zones were detected above wells where invasive interrogation has confirmed that no voids exist in the shale overburden (three wells). One well (36) appears to be influenced by the stress field from a nearby cavern.

Based upon the available downhole information, all results appear to have a reasonable match with expected (but not predicted) rock mechanics principles. Wells 6A, 26, and 94 show no shear velocity buildup, which appears to physically correlate with the absence of a significant void in the shale overburden. The cavern at well 16 shows significant buildup in shear velocity even though the void near top of salt is negligibly small. The cavern area beneath well 19/35 has previously produced a sinkhole and currently possesses a small increase in shear velocity. This is not unexpected considering the collapse of this well complex includes a significant galley structure.

For the caverns at wells 20 and 25–40, stress buildup appears smaller than might be expected for caverns of the size suggested here, while drill log and acoustic televiewer data possess evidence of multiple fractures in roof rock. These observations could be indicative of the discrete cycles that define the process of upward void migration. It is reasonable that shear velocity increases until fracturing (rupture) occurs as observed in the borehole data. This fracturing is followed by failure of roof material, reduction in shear velocity, and then upward advancement of a zone (thereby increasing shear velocity). Consistent with this suggested process, there was a roof fall at cavern 25–40 in 2011, which may have relieved some stress, leaving the observed fractures and reducing the shear velocity.

For cavern 33, significant stress buildup appears reasonable for a cavern of this size where drill log data show relatively fewer roof beam fractures. There appears to be no relevant

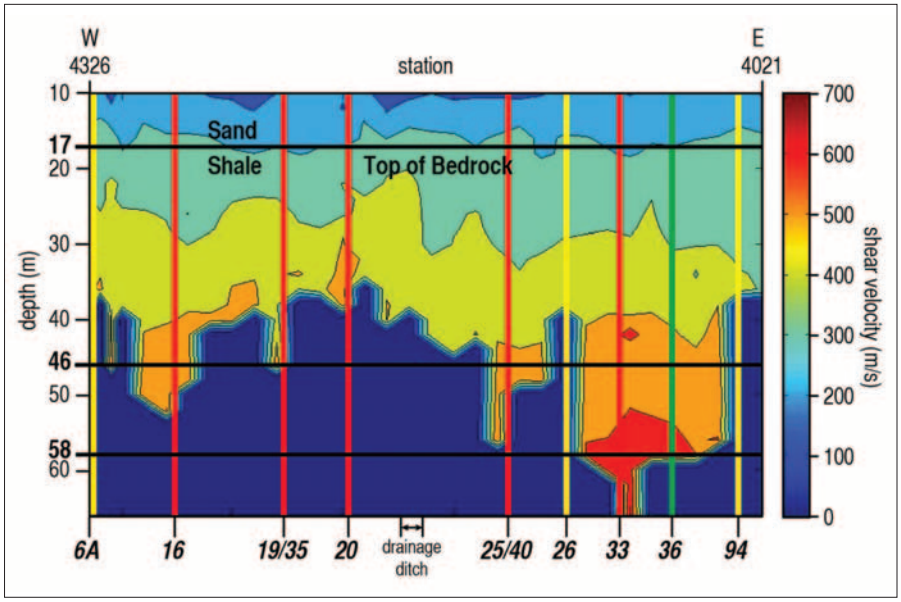

Figure 8. *Shear-wave velocity cross section of 1D passive MASW data. Vertical lines represent wells marked at the bottom horizontal axis. Red lines represent wells with voids that migrated into the shale. Yellow lines indicate wells with no voids in the shale.*

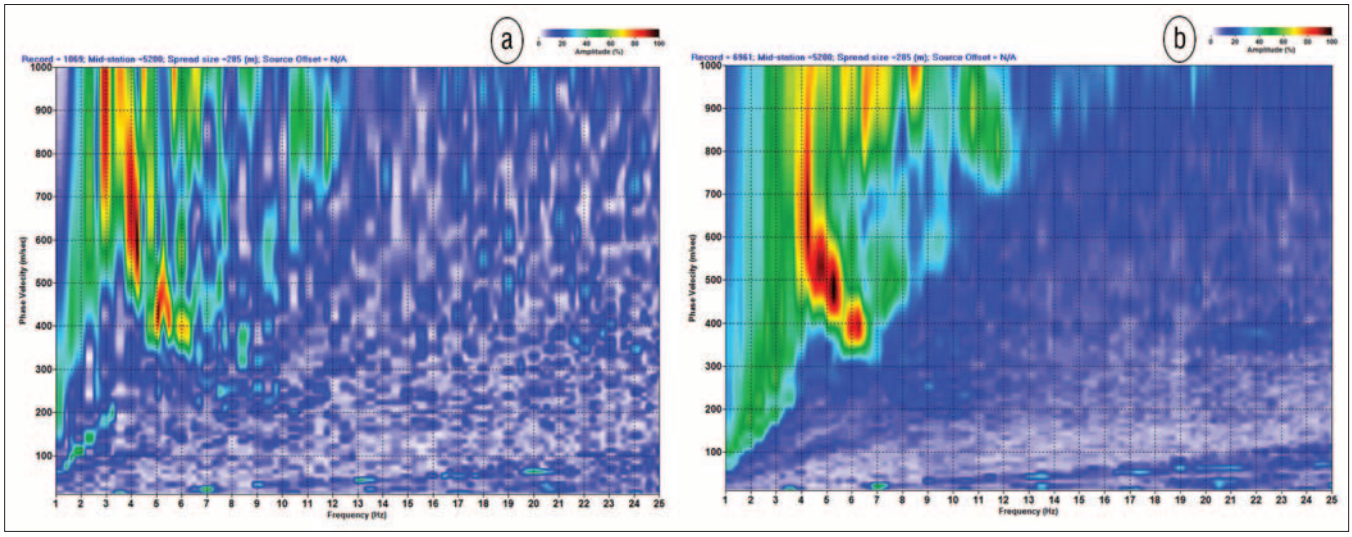

Figure 9. *Dispersion-curve imaging using (a) conventional passive-data imaging analysis and (b) analysis optimized for using trains as passive sources.*

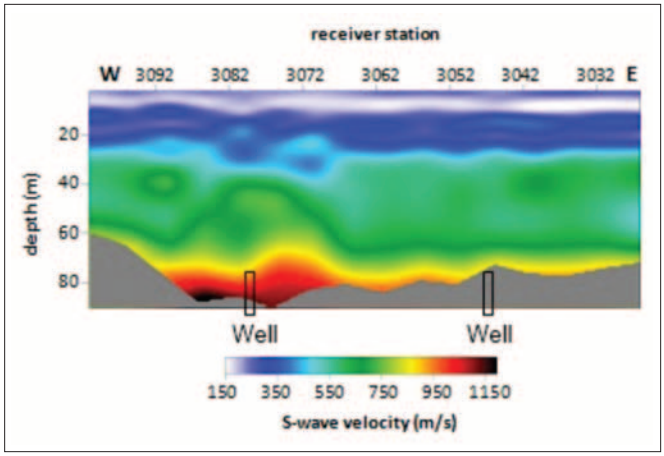

Figure 10. *A 2D V_s section showing a high V_s anomaly at one well (~station 3080) and no anomaly at another (~station 3047).*

data for well 36 because of the apparent interference of the shear-velocity field from cavern 33.

Subsequent efforts

Another set of passive MASW data were acquired at this site specifically targeting other candidate wells. This time the passive MASW dispersion-curve imaging algorithm was further optimized for analyzing trains as passive sources. This new approach was shown to be useful at providing higher-resolution dispersion-curve images (Figure 9) in comparison to the conventional imaging. This characteristic was most significant when the signal from trains was not strong.

This new survey design was successful in detecting high-velocity dome-shaped V_s anomalies (indicating elevated shear velocities) at some wells while showing no anomalies at other wells (Figure 10). The elevated shear velocity is evident and comparatively anomalous, but because of the increased sensitivity of this modification to the approach, this observed elevated shear velocity was interpreted as not large enough to suggest near-term migration of the void and associated collapse.

Conclusions

The passive MASW method as adapted to this problem appears to have detected all voids that have migrated into the shale overburden, large or small. Thus, at this point it appears the greatest risk of using this method to predict upward migration of voids is the possibility for false positives. It is unlikely a void with roof failure potential will be missed with time-lapse or monitoring type use of this method. The proposed passive MASW technique is a valid tool for prescreening old brine wells for the potential presence of cavern voids at risk of upward movement. This study showed that the passive MASW method can be successfully applied using trains as passive sources and, furthermore, and that such sources can provide even better dispersion-curve imaging than would be expected based on passive approaches currently in use. TLE

References

Davies, W. E., 1951, Mechanics of cavern breakdown: National Speleological Society, **13**, 6–43.

Louie, J. N., 2001, Faster, better: Shear-wave velocity to 100 meters depth from refraction microtremor arrays: Bulletin of the Seismological Society of America, **91**, no. 2, 347–364, http://dx.doi.org/10.1785/0120000098.

Miller, R. D., J. Xia, C. B. Park, and J. M. Ivanov, 1999, Multichannel analysis of surface waves to map bedrock: The Leading Edge, **18**, no. 12, 1392–1396, http://dx.doi.org/10.1190/1.1438226.

Park, C. B., R. D. Miller, and J. Xia, 1998, Imaging dispersion curves of surface waves on multichannel record: 68th Annual International Meeting, SEG, Expanded Abstracts, 1377–1380.

Park, C. B., R. D. Miller, J. H. Xia, and J. Ivanov, 2007, Multichannel analysis of surface waves (MASW)—active and passive methods: The Leading Edge, **26**, no. 1, 60–64, http://dx.doi.org/10.1190/1.2431832.

Xia, J. H., R. D. Miller, and C. B. Park, 1999, Estimation of near-surface shear-wave velocity by inversion of Rayleigh waves: Geophysics, **64**, no. 3, 691–700, http://dx.doi.org/10.1190/1.1444578.

Acknowledgments: We appreciate the support provided by Vigindustries Inc. and the Burns and McDonnell Engineering Company for this applied research project. We thank Rick Miller who was the driving force behind these projects. Technical assistance was provided by Brett Wedel, Brett Bennett, Bevin Bailey, Jerry Chandler, and Nathan Corbin. We appreciate Ed Lindgren's (Burns and McDonnell Engineering Company) and Jim Brand's (Vigindustries Inc.) review of this work. Assistance in manuscript preparation by Mary Brohammer greatly contributed to this work.

Corresponding author: jivanov@kgs.ku.edu